JACS
JOURNAL OF THE AMERICAN CHEMICAL SOCIETY
Article
pubs.acs.org/JACS

Transition Metal Surface Passivation Induced Graphene Edge Reconstruction

Junfeng Gao,[†,‡] Jijun Zhao,*[,†] and Feng Ding*[,‡]

[†]Key Laboratory of Materials Modification by Laser, Ion and Electron Beams, Dalian University of Technology, Ministry of Education, Dalian 116024, China

[‡]Institute of Textiles and Clothing, Hong Kong Polytechnic University, Kowloon, Hong Kong, China

Supporting Information

ABSTRACT: In vacuum, the bare zigzag (**zz**) edge of graphene is reconstructed into a line of pentagon−heptagon pairs, while the pristine armchair (**ac**) edge is retained. Our first-principle explorations of graphene edges on three metal surfaces [Cu(111), Co(111), and Ni(111)] indicate an opposite tendency, that is, the pristine **zz** edge is energetically favorable and the reconstructed **ac** edge with dangling C atoms is highly stable on Co(111) and Ni(111) surfaces. Insightful analysis shows that passivation of the graphene edge by metal surfaces is responsible for the dramatic differences. Beyond this, the unique edge configuration has a significant impact on the graphene CVD growth behavior.

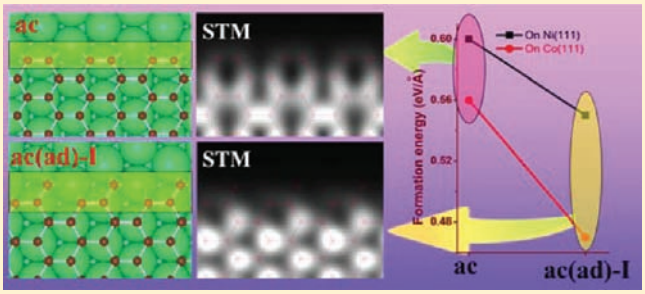

1. INTRODUCTION

Because of its outstanding electronic,[1] mechanical,[2] thermal,[3] and optical[4] properties, graphene is an ideal material for many applications. Most of the applications presuppose that graphene of high quality can be mass-produced and further tailored into devices efficiently.[5] Among the numerous methods of graphene synthesis, chemical vapor deposition (CVD) growth on transition metal (TM) surfaces stands out for its many advantages.[6] Beyond the seed nucleation stage,[7] continuous growth of graphene is a consequence of incorporation of carbon atoms onto graphene edges.[8] Hence, the formation of the graphene edge, the barrier for carbon insertion, and the configuration of growing graphene islands are crucial for both the understanding of CVD graphene growth mechanism and the guidance of experimental design.[9]

For freestanding graphene, the pristine armchair (**ac**) edge is more stable than the zigzag (**zz**) one.[10] The higher stability of the **ac** edge stems from self-passivation by the C≡C triple bonds between neighboring outermost atoms. On the contrary, a pristine **zz** edge has distinct dangling σ bonds, unpaired electrons, and thus a remarkably high formation energy. As a consequence, a freestanding graphene **zz** edge tends to be reconstructed by turning every two neighboring hexagons (6|6) on the edge into a pentagon−heptagon pair (5|7). Previous studies have showed that such "6|6 → 5|7" reconstruction can be achieved by rotating a C−C bond on the edge, and the corresponding barrier is only 0.6 eV.[10a]

During CVD growth on a TM surface, the growing graphene edges are passivated, and thus, their formation energies are considerably reduced. This may lead to different edge reconstructions and consequently affect the insertion of carbon into the graphene front and the behavior of graphene growth. In this article, we report a systematic theoretical study of graphene edge reconstruction on three typical TM surfaces for CVD growth, namely, the Co(111), Ni(111), and Cu(111) faces of their fcc crystals.[6a,11] Our study reveals that in sharp contrast to the situation in vacuum, *reconstruction with pentagons or heptagons on the edge is not favorable for graphene on TM surfaces*. The pristine **zz** edge has a lower formation energy than the reconstructed one. An unrevealed **ac**-derivative edge having an additional carbon atom attached to each armchair site is more stable than the pristine **ac** edge on Ni and Co surfaces. Moreover, the effects of these newly discovered edge structures on graphene CVD growth are discussed.

2. MODELS AND THEORETICAL METHODS

All of the calculations were performed using spin-polarized density functional theory (DFT) with the plane-wave pseudopotential technique, as implemented in the Vienna Ab Initio Simulation Package (VASP).[12] The Perdew−Burke−Ernzerhof (PBE) functional within the generalized gradient approximation (GGA) was used to describe the exchange−correlation interactions.[13] Projector-augmented wave (PAW) pseudopotentials were used to describe the core electrons.[14] The kinetic energy cutoff of 400 eV for the plane-wave basis and the convergence criterion of 10^{-4} eV were carefully tested and adopted in all of the calculations.

Co, Ni, and Cu have been extensively used as substrates in graphene epitaxial growth,[6,11a,15] and their lattices have small mismatches with that of graphene [i.e., ∼1.9% for Co(111), ∼1.1% for Ni(111), and ∼3.8% for Cu(111)].[16] These three TM surfaces were selected for our

Received: November 10, 2011
Published: March 14, 2012

dx.doi.org/10.1021/ja2104119 | J. Am. Chem. Soc. 2012, 134, 6204−6209

calculations, since it is easy to build a coperiodic lattice for graphene and the metal surface by shrinking the metal lattice slightly to fit the graphene lattice. As a compromise between accuracy and computational cost, the current scheme of structural modeling was shown to be reliable in previous work.[16] The slab model of each TM substrate included three layers of atoms, with the bottom layer fixed. An orthorhombic cell of graphene was chosen, with optimized lattice constants a = 4.264 Å and b = 2.462 Å.

TM-supported graphene nanoribbons (GNRs) with two equal edges were used to model the graphene edges. For **ac**-derivative edges, a (2 × 9) supercell was used with a mesh of 5 × 2 **k** points. Ten pristine armchair rows were put on the metal surface, with the middle four C rows kept in the same plane to simulate infinite graphene. A (6 × 2) supercell was adopted for **zz**-derivative edges with a mesh of 9 × 2 **k** points, and eight rows of **zz** chains were put on the metal surface with the middle two rows kept at the same height. The total energy converged to less than 1 meV/atom with the present choice of **k** points. The distances between the two edges of a GNR or two neighboring GNRs were greater than 1 nm to ensure that the edge−edge interaction was negligible. To mimic the formation of infinite graphene on the TM surface, as shown in Figure 1f, the height of a few middle rows of atoms in the GNR was fixed at the value for infinite graphene on the TM surface [2.2, 2.3, and 3.1 Å for Co, Ni, and Cu, respectively; see sections S2 and S4 in the Supporting Information (SI) for a detailed assessment of the choices of height and GGA method used in this study].[16]

Instead of a global search, the edge configurations investigated here were obtained by adding carbon atoms to the edge or rotating one C−C bond directly. Among the possible edges considered (see section S1 in the SI), six most probable ones are discussed since they are relatively more stable, as were also found in previous studies of free-standing edges.[10] The relative stability of a graphene edge can be characterized by its formation energy E_f, defined as:

$$E_f = \frac{E_t - N\varepsilon_g - E_{TM}}{2l} \quad (1)$$

where E_t is the total energy of the graphene−TM system, N is the number of C atoms, ε_g is the energy of graphene per C atom, E_{TM} is the energy of the TM substrate, l is the length along the ribbon edge, and the factor of 2 accounts for the two identical edges on the metal terraces.

For continuous growth of high-quality graphene, it is necessary to transform the possible **zz(57)** edges to pristine **zz** edges in order to avoid 5|7 defects. To estimate the energy barrier, the climb-nudged elastic band method[17] was used to search the transition states and locate possible intermediate configurations for the **zz** → **zz(57)** transformation on the Co, Ni, and Cu substrates and in vacuum. The supercell dimensions of **zz** and **zz(57)** on the TM surface and in vacuum were set as 4.92 Å × 21.30 Å × 25 Å, which included two **zz** periods. The graphene ribbon had a width of six zigzag rows; one side was passivated by hydrogen, and the **zz** → **zz(57)** transition occurred on the other side.

3. RESULTS AND DISCUSSION

Some of the considered configurations of graphene edges on TM surfaces are shown in Figure 1, and the others are shown in Figure S1 in the SI. Among them, the **zz(57)**/**ac(677)** edge can be achieved by rotating a C−C bond on the pristine **zz**/**ac** edge, and the **ac(ad)**/**zz(ad)** edge can be obtained by adding one C atom to each unit cell of the pristine **ac**/**zz** edge. Interestingly, the **ac(ad)** edge on the TM surfaces shows two distinctly different geometries. On Cu(111), the additional C atom bonds to both edge C atoms of the armchair site to form a pentagon [see **ac(ad)-II** in Figure 1g], similar to the previously reported freestanding **ac(56)** edge.[10a,b] However, on both Ni(111) and Co(111) surfaces, the C adatom bonds only to one of the edge C atoms, presenting an unrevealed edge

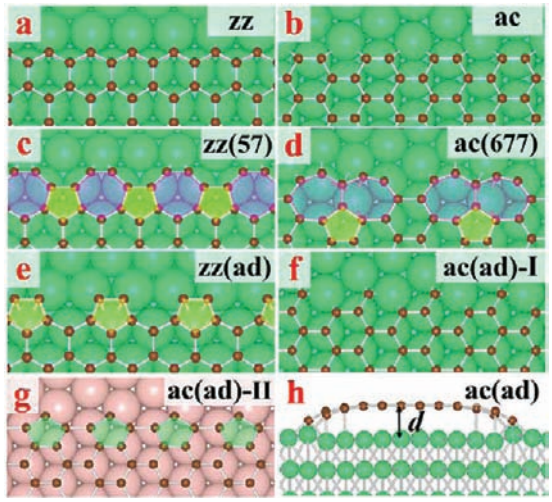

Figure 1. Some typical supported graphene edges on TM surfaces. (a−g) Top views of (a) pristine **zz** edge; (b) pristine **ac** edge; (c) reconstructed **zz(57)** edge; (d) reconstructed **ac(677)** edge; (e) reconstructed **zz**(ad) edge formed from **zz** with one additional carbon atom on each edge atom; and two configurations of the **ac** edge with one additional atom on each armchair site: (f) **ac(ad)-I** on Co(111) and (g) **ac(ad)-II** on Cu(111). (h) Side view of the **ac(ad)-I** edge on Co(111).

geometry [i.e., **ac(ad)-I** in Figure 1f]. In the following discussions, we will show that **ac(ad)-I** is a very stable graphene edge configuration on both Ni(111) and Co(111).

The formation energies for all of the explored edges are summarized in Table S2 in the SI and plotted in Figure 2.

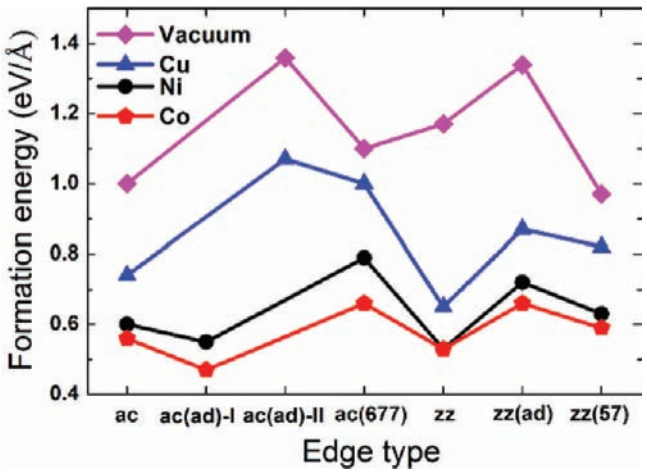

Figure 2. Formation energies for various graphene edges in vacuum and on TM surfaces.

Clearly, the formation energies for all of the graphene edges on TM surfaces are significantly lower than those in vacuum as a result of passivation by the metal surface. On both the Co(111) and Ni(111) surfaces, the average formation energy drops by ∼50%, while the energy reduction on Cu(111) is only 30%, which indicates that Co and Ni passivate the graphene edge more efficiently than Cu. More importantly, the energy drops are configuration-dependent, and thus, the order of their formation energies has also been changed. In short, *edge reconstruction on TM surfaces is different from that in vacuum.*

dx.doi.org/10.1021/ja2104119 | *J. Am. Chem. Soc.* 2012, 134, 6204−6209

Among the three configurations derived from **zz** edges, either on the TM surfaces or in vacuum, the **zz(ad)** edge has the highest formation energy and thus is not a stable structure during graphene CVD growth.[10d,18] The **zz(57)** configuration, which is the most stable **zz** edge in vacuum,[10a] has a higher formation energy than the pristine **zz** edge on all the three TM surfaces. Therefore, our calculations indicate that in sharp contrast to the situation in vacuum, *there is no reconstruction of the zz graphene edge on TM surfaces.*[19] To provide further verification of this conclusion, we calculated the formation energies of the **zz** and **zz(57)** edges on the Rh(111) surface and obtained the exact same result (see section S3 in the SI). For the three explored **ac**-derivative edges, the pristine one still has the lowest formation energy on the Cu(111) surface, but the **ac(ad)-I** edge is more energetically favorable on both Ni(111) and Co(111).

Certainly, as the only external factor, metal passivation must be responsible for these differences. On a TM surface, the edge C atoms of the pristine graphene edge are passivated by the free electrons of the metal (Figure 3g,h). This leads to a significant decrease in the formation energies (Figure 2) as well as curved-down configurations of the graphene edges (Figure 1h). For example, the formation energy for the **zz** edge drops by 45−60%, from 1.17 eV/Å in vacuum to 0.53 eV/Å on the Co or Ni surface and 0.65 eV/Å on the Cu surface. Although edge reconstructions such as "6|6 → 5|7" may further reduce the formation energy of the outermost C atoms by forming very stable C≡C triple bonds,[10a] it creates nonhexagonal polygons with high intrinsic formation energies. Hence, we conclude that *on metal surfaces, these graphene edges do not intend to incorporate any nonhexagonal polygons*. As evidence of this, Figure 2 shows that all of the edges with pentagons or heptagons [e.g., **zz(57)**, **zz(ad)**, and **ac(677)**] possess very high formation energies.

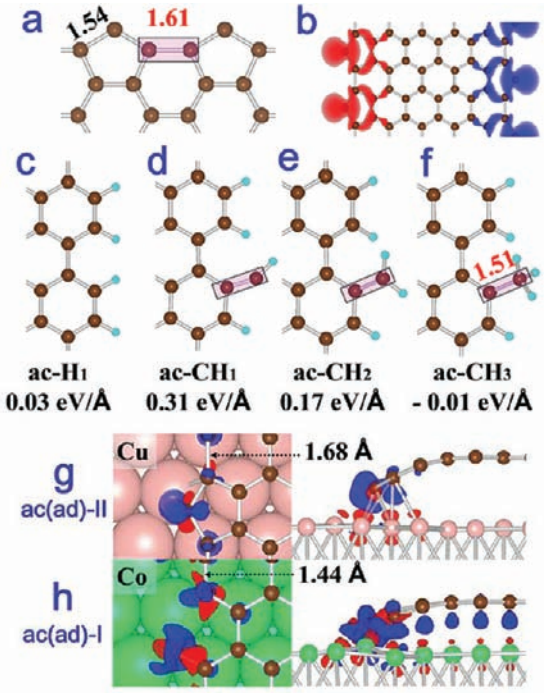

Figure 3. (a) The **ac(ad)-II** [or **ac(56)**] edge in vacuum. (b) Spin densities of the free-standing **ac(ad)-II** edge. (c−f) Various **ac** edges terminated by H or CH_n (n = 1−3) groups along with their formation energies, which are defined with respect to the energies of the C atom in graphene and the H atom in H_2. (g, h) Charge difference distributions for (g) the **ac(ad)-II** edge on the Cu surface and (h) the **ac(ad)-I** edge on the Co surface, in which blue zones indicate gain of charge and red zones loss of charge.

Surprisingly, the **ac(ad)-I** edge with a dangling C atom bonded to only one of the two edge atoms of each **ac** site is the most stable configuration among the **ac**-derivative edges on the Ni and Co surfaces. In vacuum, this additional C atom of the **ac(ad)** edge tends to passivate two edge carbon atoms, forming a pentagon at each **ac** site (Figure 3a). Although the number of edge atoms (those with two or fewer C neighbors) is reduced by 50%, such an edge configuration is rather energetically unfavorable because of the highly stretched C−C bonds on the edge (Figure 3a) and the unpaired π electron on each edge atom (Figure 3b).[10a] The freestanding **ac(ad)** formation can be stabilized by opening one edge of the pentagon (or forming an incomplete hexagon) and passivating the dangling edge atoms with hydrogen. Here we terminated the additional C atom with one to three hydrogen atoms, creating CH_n (n = 1−3) groups at the edge (Figure 3d−f). Among these three passivations, the freestanding **ac-CH_3** edge has the lowest formation energy, suggesting that the outermost C atoms prefer sp^3 hybridization. The outermost C−C bond, whose length is 1.51 Å, corresponds to a single bond. It is important to note that the formation energy of the **ac-CH_3** edge is even lower than that of the H-passivated pristine **ac** edge (Figure 3c) by 0.04 eV/Å or 0.17 eV per **ac** site.

When the **ac(ad)-I** edge is placed on the Ni or Co surface, the very active outermost C atom is passivated by the TM surface. As shown in Figure 3h, the additional C atom bends toward the metal surface and interacts strongly with three metal atoms. This passivation significantly stabilizes the outermost C(sp^3) atom, leading to a remarkable reduction in the edge formation energy by ∼0.9 eV/Å (Figure 2), which is about twice the energy drop for the pristine **ac** edge. Consequently, the **ac(ad)-I** edge prevails over the pristine **ac** edge on both the Co and Ni surfaces.

It is known that the Cu(111) surface has a much weaker affiliation with carbon atoms.[16a] On the Cu(111) surface, as in vacuum, the **ac(ad)-I** configuration is not stable and transforms into **ac(ad)-II** upon optimization. The energy reduction for **ac(ad)-II** due to Cu passivation is 0.29 eV/Å, which is only one-third of that for **ac(ad)-I** on the Ni and Co surfaces. Moreover, the C−C bond linking two pentagons is as long as 1.68 Å (Figure 3g), implying a very high local strain (18.2%) with respect to the standard C(sp^2)−C(sp^2) bond length. Therefore, the weak interaction between the carbon atom and Cu(111) surface as well as the large edge strain are responsible for the lower stability of the **ac(ad)-II** edges on Cu. The difference between the Cu and Co/Ni substrates can be also seen by the charge difference distributions in Figure 3g,h, which show a more pronounced interaction between the Co surface and the graphene atoms.

To provide further evidence for the unrevealed **ac(ad)-I** edge, we simulated its STM images on the Ni(111) and Co(111) surfaces and compared them with those for the **ac** edge (Figure 4). It is hard to see the outermost C atoms of the **ac(ad)-I** edge clearly because they stay too close to the metal surface and are submerged by electrons from the metal atoms. Noticeably, the STM images of the **ac** and **ac(ad)-I** edges show distinct differences. The inner carbon atoms of the **ac(ad)-I** edge retain the threefold symmetry, presenting three bright spots per six-membered ring (Figure 4a,c), while the pristine **ac**

dx.doi.org/10.1021/ja2104119 | J. Am. Chem. Soc. 2012, 134, 6204−6209

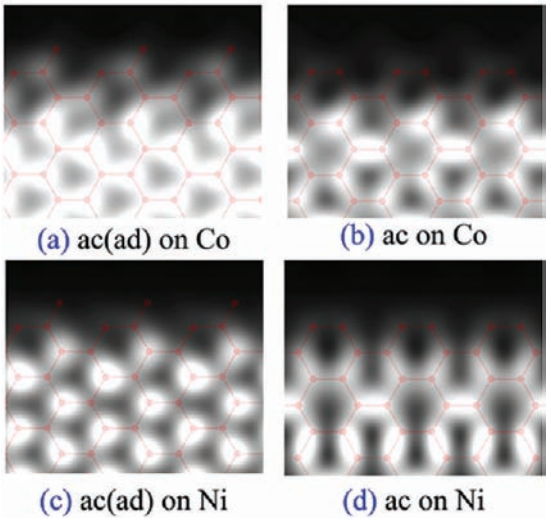

Figure 4. Simulated STM images of the **ac** and **ac(ad)** edges on Ni and Co surfaces obtained using the Tersoff–Hamann approximation.[20] The bias was −200 mV. (a) **ac(ad)-I** edge on the Co(111) surface; (b) **ac** edge on the Co(111) surface; (c) **ac(ad)-I** edge on the Ni(111) surface; (d) **ac** edge on the Ni(111) surface. The STM tip heights relative to the top atom of system were greater than 2 Å and kept constant during calculations.

edge with broken symmetry exhibits totally different patterned images (Figure 4b,d).

To examine ulteriorly the stability of the **ac(ad)-I** edges on the TM surfaces, we performed ab initio molecular dynamics (MD) simulations within the canonical ensemble (using the algorithm of Nosé[8,9]) for the **ac(ad)-I** edge on the Co(111) surface (details are given in section S5; also see the movie in the SI). In the 2.5 ps MD simulation at 800 K, the **ac(ad)-I** edge shows exceptional stability, and no noticeable structural deformation or bond reconstruction is seen.

According to our geometry optimization results, the transitions between **ac(ad)-I** and **ac(ad)-II** on Co, Ni, and Cu are spontaneous, without any energy barrier. However, for the **zz** → **zz(57)** transition, there is a barrier originating from the C–C bond rotation. Using climb-nudged elastic band methods,[17] we searched for the transition barrier and possible intermediate states for the **zz** → **zz(57)** transitions in vacuum and on Co, Ni, and Cu. In vacuum, the barrier for the **zz** → **zz(57)** transition [where the antiferromagnetic **zz** edge transforms to the nonmagnetic **zz(57)** edge] is ∼1.23 eV (0.56 eV without the spin polarization calculation, in agreement with the value of 0.6 eV reported in ref 10a), and the reverse barrier for the **zz(57)** → **zz** transition is 2.27 eV (2.4 eV in ref 10a). On the TM surfaces, the **zz** → **zz(57)** transition barriers are remarkably larger: 2.06 eV on Co, 2.93 eV on Ni, and 3.18 eV on Cu. The reverse barriers for the **zz(57)** → **zz** transition are 1.40 eV on Co, 1.92 eV on Ni, and 2.01 eV on Cu, respectively. The increased barrier can be understood by the fact that the **zz** and **zz(57)** edges (as the initial and final states) on the TM surfaces are much more stable than the freestanding ones. Indeed, on a metal surface with weak interactions (e.g., Cu), the transition mechanism is similar to that in vacuum. In contrast, on strongly interacting surfaces (e.g., Co and Ni), the transition mechanism is rather different, as it involves an intermediate state (see Figure 5). To synthesize high-quality graphene, transforming **zz(57)** edges into **zz** edges is important. On the basis of the above transition barriers, we

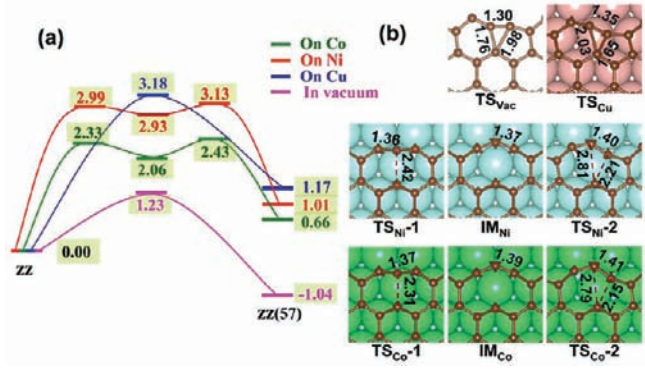

Figure 5. (a) Transition barriers (eV/unit) and reaction paths of **zz**–**zz(57)** transitions in vacuum and on Co, Ni, and Cu. (b) Geometries of transition states (TS) and intermediates (IM) for the transitions in vacuum and on Co, Ni, and Cu.

can estimate the average transition time as $\tau = (h/k_BT) \times \exp(E^*/k_BT)$, where k_B and h are Boltzmann's and Planck's constants, respectively, T is the absolute temperature, and E^* is the total energy barrier (shown in Figure 5a). At 1000 K, which is a conventional temperature for growth of graphene by CVD, the average ratios for the **zz(57)** → **zz** transition are about 2.0 × 10^6 s^{-1} on Co, 5.0 × 10^3 s^{-1} on Ni, and 1.7 × 10^3 s^{-1} on Cu, which are sufficient for graphene growth in realistic situations.

Having clarified the graphene edge configurations and their formation energies on the TM surfaces, we now turn to their effects on the graphene growth behavior. First, they affect the equilibrium morphologies of TM-supported graphene islands and the edges exposed on the front of a growing graphene patch. Figure 6 presents the equilibrium shapes of graphene

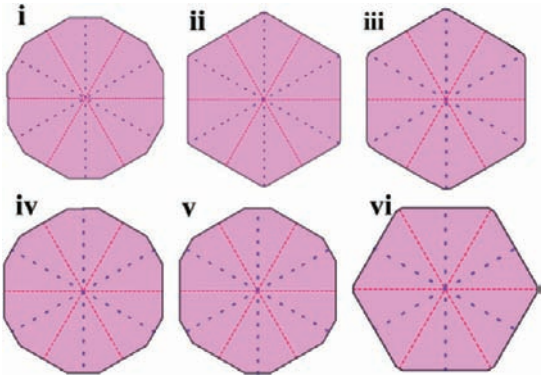

Figure 6. Wulff shapes of graphene flakes in the equilibrium state: (i) freestanding flake with **ac** and **zz(57)** edges; (ii) flake on Cu with only pristine **ac** and **zz** edges; (iii, iv) flakes on Ni with (iii) **ac** and **zz** edges and (iv) **ac(ad)** and **zz** edges; (v, vi) flakes on Co with (v) **ac** and **zz** edges and (vi) **ac(ad)** and **zz** edges. Red dashed lines represent the **zz** direction and blue dotted lines the **ac** direction.

patches explored by the Wulff construction.[21] On the Cu and Co surfaces, an equilibrium graphene island grown with energetically preferential edges exhibits a hexagonal shape, which is the same as those experimentally observed on Cu.[22] In contrast, the equilibrium shape of a graphene flake on the Ni surface is a dodecagon. This is very similar to the observation that the equilibrium shapes of graphene flakes can be greatly altered by different H termination.[9]

Second, the details of C insertion into the front of a growing graphene patch must depend on the edge configuration. Figure

dx.doi.org/10.1021/ja2104119 | J. Am. Chem. Soc. 2012, 134, 6204–6209

7 shows the processes of adding two C atoms to the pristine **ac** edges on the Cu, Ni, and Co surfaces. On Cu(111), a carbon

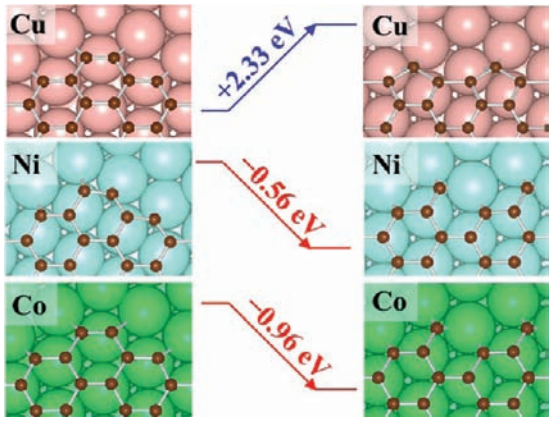

Figure 7. Different processes for adding two C atoms to pristine **ac** graphene edges on Cu(111), Ni(111), and Co(111) surfaces and their relative formation energies.

dimer has a much lower formation energy than a monomer,[23] and thus, the addition of C atoms should occur in the form of dimers. After a C_2 dimer diffuses to an **ac** site and forms a hexagon on the pristine **ac** edge, the second hexagon then forms at an adjacent **ac** site by insertion of another C_2 dimer. In this way, more and more hexagons grow on the **ac** edge until a complete line of hexagons comes into being and hence pushes the graphene front one step forward; this resembles the process of carbon nanotube growth near a metal step of the catalyst particle.[8a] Meanwhile, the **ac(ad)** edge on Cu is less stable than the pristine **ac** edge by 0.33 eV/Å or 1.41 eV per **ac** site, so it is energetically unfavorable in the graphene growth process.

The growth behavior of the **ac** edges on the Ni and Co surfaces is markedly different from that on Cu. It is known that C monomers and dimers have very similar formation energies on the Ni(111) and Co(111) surfaces.[23] As shown in Figure 7, the C adatoms on the pristine **ac** edge form **ac(ad)-I** edges instead of hexagons. Because the **ac(ad)-I** edge is the most energetically preferred structure on the Ni(111) and Co(111) surfaces along the armchair orientation, the growing **ac** edge tends to maintain the **ac(ad)-I** configuration. When a C monomer diffuses to an **ac(ad)-I** site and forms a hexagon, a new **ac** edge is created locally. The subsequent C atom then preferentially attaches to the new **ac** site, transforming the **ac** edge back into an **ac(ad)-I** edge. When a C_2 dimer diffuses to an **ac(ad)-I** edge, a local **ac(ad)-I** edge is formed directly.

It should be noted that hydrogen may also plays an important role in graphene CVD growth, as most feedstocks used in graphene synthesis are hydrocarbon molecules. In graphene growth by CVD, a graphene edge may be terminated by either H or the metal surface. Relative to the H- terminated graphene edges, the metal-passivated ones are more active. Thus, the incorporation of C atoms in graphene growth is very likely to occur on the metal-passivated edges.

4. CONCLUSIONS

In essence, a variety of graphene edges on Cu(111), Ni(111), and Co(111) surfaces have been explored computationally. In sharp contrast to the freestanding graphene edges, the reconstructed edges with pentagons and heptagons are not stable on transition metal surfaces as a result of passivation of the graphene edge by the metal. An unexpected **ac(ad)-I** configuration with dangling C atoms is the most stable armchair edge on strong interaction metal surfaces (Co, Ni). The difference in the **ac** and **ac(ad)-I** edges on metal surfaces might be identified by their STM images. Beyond this, the equilibrium shapes of graphene flakes and the C addition process in graphene growth on Cu(111), Ni(111), and Co(111) surfaces are greatly affected by the substrate-dependent edge reconstruction.

■ ASSOCIATED CONTENT

Supporting Information

Complete optimized structures of graphene edges on Co(111), Ni(111), and Cu(111) surfaces; table of formation energies in detail for all of the explored edges both in vacuum (compared with previous results) and on the three TM surfaces; and complete refs 6a and 22. This material is available free of charge via the Internet at http://pubs.acs.org.

■ AUTHOR INFORMATION

Corresponding Author

zhaojj@dlut.edu.cn; feng.ding@rice.edu

Notes

The authors declare no competing financial interest.

■ ACKNOWLEDGMENTS

This work was supported by the National Natural Science Foundation of China (11134005) and the Program for Changjiang Scholars and Innovative Research Team in University of China.

■ REFERENCES

(1) (a) Novoselov, K. S.; Geim, A. K.; Morozov, S. V.; Jiang, D.; Zhang, Y.; Dubonos, S. V.; Grigorieva, I. V.; Firsov, A. A. *Science* **2004**, *306*, 666. (b) Castro Neto, A. H.; Guinea, F.; Peres, N. M. R.; Novoselov, K. S.; Geim, A. K. *Rev. Mod. Phys.* **2009**, *81*, 109.

(2) Lee, C.; Wei, X.; Kysar, J. W.; Hone, J. *Science* **2008**, *321*, 385.

(3) Balandin, A. A.; Ghosh, S.; Bao, W.; Calizo, I.; Teweldebrhan, D.; Miao, F.; Lau, C. N. *Nano Lett.* **2008**, *8*, 902.

(4) Liu, M.; Yin, X.; Ulin-Avila, E.; Geng, B.; Zentgraf, T.; Ju, L.; Wang, F.; Zhang, X. *Nature* **2011**, *474*, 64.

(5) (a) Geim, A. K. *Science* **2009**, *324*, 1530. (b) Geim, A. K.; Novoselov, K. S. *Nat. Mater.* **2007**, *6*, 183.

(6) (a) Bae, S.; et al. *Nat. Nanotechnol.* **2010**, *5*, 574. (b) Li, X.; Cai, W.; An, J.; Kim, S.; Nah, J.; Yang, D.; Piner, R.; Velamakanni, A.; Jung, I.; Tutuc, E.; Banerjee, S. K.; Colombo, L.; Ruoff, R. S. *Science* **2009**, *324*, 1312.

(7) (a) Gao, J.; Yip, J.; Zhao, J.; Yakobson, B. I.; Ding, F. *J. Am. Chem. Soc.* **2011**, *133*, 5009. (b) Gao, J.; Yuan, Q.; Hu, H.; Zhao, J.; Ding, F. *J. Phys. Chem. C* **2011**, *115*, 17695.

(8) (a) Ding, F.; Harutyunyan, A. R.; Yakobson, B. I. *Proc. Natl. Acad. Sci. U.S.A.* **2009**, *106*, 2506. (b) Loginova, E.; Bartelt, N. C.; Feibelman, P. J.; McCarty, K. F. *New J. Phys.* **2008**, *10*, No. 093026.

(9) Gan, C. K.; Srolovitz, D. J. *Phys. Rev. B* **2010**, *81*, No. 125445.

(10) (a) Koskinen, P.; Malola, S.; Häkkinen, H. *Phys. Rev. Lett.* **2008**, *101*, No. 115502. (b) Wassmann, T.; Seitsonen, A. P.; Saitta, A. M.; Lazzeri, M.; Mauri, F. *Phys. Rev. Lett.* **2008**, *101*, No. 096402. (c) Kroes, J. M. H.; Akhukov, M. A.; Los, J. H.; Pineau, N.; Fasolino, A. *Phys. Rev. B* **2011**, *83*, No. 165411. (d) Ivanovskaya, V. V.; Zobelli, A.; Wagner, P.; Heggie, M. I.; Briddon, P. R.; Rayson, M. J.; Ewels, C. P. *Phys. Rev. Lett.* **2011**, *107*, No. 065502.

(11) (a) Eom, D.; Prezzi, D.; Rim, K. T.; Zhou, H.; Lefenfeld, M.; Xiao, S.; Nuckolls, C.; Hybertsen, M. S.; Heinz, T. F.; Flynn, G. W. *Nano Lett.* **2009**, *9*, 2844. (b) Kim, K. S.; Zhao, Y.; Jang, H.; Lee, S. Y.;

Kim, J. M.; Kim, K. S.; Ahn, J.-H.; Kim, P.; Choi, J.-Y.; Hong, B. H. *Nature* **2009**, *457*, 706.
(12) (a) Kresse, G.; Furthmüller, J. *Phys. Rev. B* **1996**, *54*, 11169. (b) Kresse, G.; Furthmüller, J. *Comput. Mater. Sci.* **1996**, *6*, 15.
(13) Perdew, J. P.; Burke, K.; Ernzerhof, M. *Phys. Rev. Lett.* **1996**, *77*, 3865.
(14) (a) Blöchl, P. E. *Phys. Rev. B* **1994**, *50*, 17953. (b) Kresse, G.; Joubert, D. *Phys. Rev. B* **1999**, *59*, 1758.
(15) (a) Ramón, M. E.; Gupta, A.; Corbet, C.; Ferrer, D. A.; Movva, H. C. P.; Carpenter, G.; Colombo, L.; Bourianoff, G.; Doczy, M.; Akinwande, D.; Tutuc, E.; Banerjee, S. K. *ACS Nano* **2011**, *5*, 7198. (b) Dedkov, Y. S.; Fonin, M.; Rüdiger, U.; Laubschat, C. *Phys. Rev. Lett.* **2008**, *100*, No. 107602.
(16) (a) Giovannetti, G.; Khomyakov, P. A.; Brocks, G.; Karpan, V. M.; van den Brink, J.; Kelly, P. J. *Phys. Rev. Lett.* **2008**, *101*, No. 026803. (b) Khomyakov, P. A.; Giovannetti, G.; Rusu, P. C.; Brocks, G.; van den Brink, J.; Kelly, P. J. *Phys. Rev. B* **2009**, *79*, No. 195425.
(17) (a) Mills, G.; Jónsson, H.; Schenter, G. K. *Surf. Sci.* **1995**, *324*, 305. (b) Sheppard, D.; Terrell, R.; Henkelman, G. *J. Chem. Phys.* **2008**, *128*, No. 134106.
(18) Suenaga, K.; Koshino, M. *Nature* **2010**, *468*, 1088.
(19) (a) Phark, S.-h.; Borme, J.; Vanegas, A. L.; Corbetta, M.; Sander, D.; Kirschner, J. *ACS Nano* **2011**, *5*, 8162. (b) Subramaniam, D.; Libisch, F.; Li, Y.; Pauly, C.; Geringer, V.; Reiter, R.; Mashoff, T.; Liebmann, M.; Burgdörfer, J.; Busse, C.; Michely, T.; Mazzarello, R.; Pratzer, M.; Morgenstern, M. *Phys. Rev. Lett.* **2012**, *108*, No. 046801.
(20) Tersoff, J.; Hamann, D. R. *Phys. Rev. Lett.* **1983**, *50*, 1998.
(21) Markov, I. V. *Crystal Growth for Beginners: Fundamentals of Nucleation, Crystal Growth and Epitaxy*, 2nd ed.; World Scientific: Singapore, 2003.
(22) Yu, Q.; et al. *Nat. Mater.* **2011**, *10*, 443.
(23) Chen, H.; Zhu, W.; Zhang, Z. *Phys. Rev. Lett.* **2010**, *104*, No. 186101.